ЖЭТФ, 2014, том 146, вып. 3 (9), стр. 607–617

CRYSTAL AND MAGNETIC PROPERTIES OF THE NEW COPPER–SODIUM BORATE $CuNaB_3O_6 \cdot 0.842H_2O$

A. M. Vorotynov [a]*, ***A. N. Vasiliev*** [a], ***V. V. Rudenko*** [a], ***O. A. Bayukov*** [a], ***D. A. Velikanov*** [a], ***S. G. Ovchinnikov*** [a], ***O. V. Vorotynova*** [b]

[a] *Kirensky Institute of Physics, SB RAS*
660036, Krasnoyarsk, Russia

[b] *Siberian Federal University*
660041, Krasnoyarsk, Russia

Received April 2, 2014

A new compound $CuNaB_3O_6 \cdot 0.842H_2O$ was grown for the first time. Its crystal structure, magnetic susceptibility, and magnetic resonance properties are presented. It was proposed that $CuNaB_3O_6 \cdot 0.842H_2O$ is a spin-Peierls magnet with the transition temperature $T_{SP} \sim 128$ K and a ladder spin structure. The possibility of a structure phase transition at $T < T_{SP}$ is predicted.

DOI: 10.7868/S004445101409020X

1. INTRODUCTION

Search for and investigations of new materials with specific magnetic and electric properties are among high-priority directions in the development of physics of magnetism and solid state physics. Great interest in exploring new systems is connected with the solution of some fundamental problems of physics, including physics of magnetic phenomena. In particular, compounds of copper ions are very interesting from this standpoint. Cuprates with spin $S = 1/2$, as a separate class of compounds, are interesting magnets with different magnetic structures, which are characterized by different magnetic dimensionality and low-temperature quantum effects. Metagermanat $CuGeO_3$ investigated by us was the first example of an inorganic spin-Peierls compound [1–3], $LiCu_2O_2$ was a chain antiferromagnet with broken ladder magnetic structure [4], Bi_2CuO_4, a 3D antiferromagnet with four-spin exchange interaction [5], and $CuGa_2O_4$, a spin glass state compound [6]. In continuation of this work, single crystals $CuNaB_3O_6 \cdot 0.842H_2O$ were grown for the first time in the system $SrO–CuO–B_2O_3–Na_2B_4O_7–H_2O$. The results of the investigation of their magnetic and resonance properties are presented for the first time.

*E-mail: sasa@iph.krasn.ru

2. SAMPLE PREPARATION

Single crystals of the compound $CuNaB_3O_6 \cdot 0.842H_2O$ were grown in the system $SrO–CuO–B_2O_3–Na_2B_4O_7–H_2O$. The technological process can be divided into three stages:

1. The original composition of $Sr(NO_3)_2$ (17.3 weight %), CuO (43 weight %), and H_3BO_3 (39.7 weight %) after grinding was annealed in a crucible during 24 hours at $T = 850\,^\circ$C. Such annealing is necessary for at least three times in order to produce a dark-green polycrystalline phase.

2. Reagents $Sr(NO_3)_2$ (4.2 weight %), CuO (10.3 weight %), B_2O_3 (5.4 weight %), and $Na_2B_4O_7$ (77.0 weight %) and the synthesized polycrystalline phase (3.1 weight %) were melted in a Pt crucible located in the furnace. After dissolution of the reagents, the temperature was decreased to 740 °C and the melt was mixed up.

3. Then the cooled mixer and the crucible were located in a glass with hot water and dissolution of the melt occurred. After cooling, glass crystals in the form of needles of dark-blue color up to 1.5 mm in length dropped out.

Table 1. Experimental data and structure refinement parameters

Formula	$CuNaB_3O_6 \cdot 0.842H_2O$
Molecular weight	232.98
Temperature, K	298
Space group	$P2_1/c$
Z	4
$2\theta_{max}$	57°
a, b, c, Å	3.4924(4), 13.428(1), 11.609(1)
β	96.822(1)°
V, Å^3	540.6(1)
ρ, g/cm^3	2.863
μ, mm^{-1}	4.103
Number of peaks	4929
Independent peaks	1364
Number of peaks with $F > 4\sigma_F$	1185
h, k, l limts	$-4 \le h \le 4$, $-18 \le k \le 17$, $-15 \le l \le 15$
Refinement results	
Weight refinement on F^2	$w = [\sigma^2 + (0.029P)^2 + 0.35P]^{-1}$, $P = (F_o^2 + 2F_c^2)/3$
Number of the refinement parameters	111
$R1[F_o > 4\sigma(F_o)]$	0.0253
$wR2$	0.0608
GooF	1.071
The extinction parameter	0.0016(9)
$(\Delta\rho)_{max}$, e/Å^3	0.43
$(\Delta\rho)_{min}$, e/Å^3	−0.37
$(\Delta/\sigma)_{max}$	0.00

3. CRYSTAL STRUCTURE

Experimental diffraction data were collected from a prismatic form single crystal with dimensions $0.126 \times \times 0.124 \times 0.374$ mm^3 by using single crystal X-ray autodiffractometer SMART APEX II with a CCD detector (Bruker AXS), MoK$_\alpha$-radiation. Corrections for absorption are entered on the basis of their calculation by the multi-scan method (SAINT) [7]. Because the initial total formula of the sample was not known, it was determined in the course of searching for the model and its refinement. As a result, all atoms of the compound were identified and located, including an unexpected water molecule. The positions of nonhydrogen atoms were refined in the anisotropic approximation of thermal fluctuations and hydrogen atoms of water that were allocated from the electron density difference syntheses were further specified in the fixed condition (rider model). It turned out that refinement of the fill factor (sof) of the water position lowers the R-factor

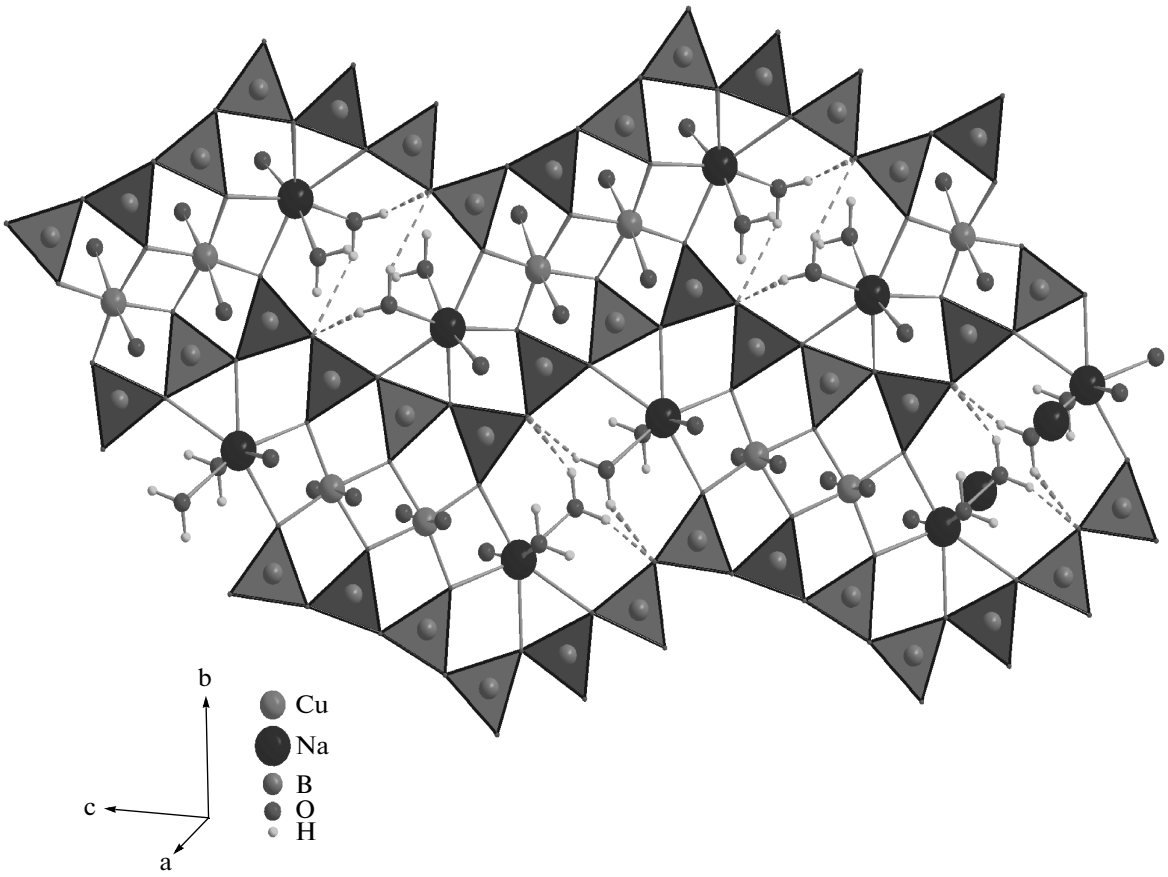

Fig. 1. Stacking of the structural blocks in the $CuNaB_3O_6 \cdot 0.842H_2O$ crystal

down to 0.2 % and leads to the value sof = 0.842 (7). All calculations were performed with the assistance of the complex SHELXTL [8]. Crystallographic experimental data and refinement parameters are presented in Table 1.

The structure is built primarily of endless zigzag chains of VO_3 triangles, where links of triangles from atoms B1, B2, and B_3 are repeated with 180° rotation for the triangles. The triangles are connected by shared vertices O1 and O2, and links by O6 vertices (Fig. 1).

The planes passing through adjacent chains are parallel to each other and coincide in orientation with a package of the crystallographic planes $(\bar{1}02)$, deviating from them by ±0.45 Å. Because the interplane distance is here equal to 3.141 Å, the plane chains are broken into pairs with distance 0.9 Å in a pair (Fig. 2).

The metal ions are located only between pair planes with the deviation from the plain $(\bar{1}02)$ about ±0.03 Å for Cu^{2+}, and ±0.25 Å for Na^+ (see Fig. 3).

The copper polyhedron CuO_6 consists of the oxygen atoms O3, O4, $O4^i$, and O5 that are situated at four vertices (O_4 atoms are connected by the symmetry center) and are common with BO_3 triangles from a chain pair (see Fig. 1). The Cu–O distances here vary from 1.919 to 1.939(2) Å. The other two oxygen ions $O4^{ii}$ and $O5^{iii}$ are common with the triangles from a neighboring chain pair. The Cu–$O4^{ii}$ distance is equal to 2.781(2) Å and Cu–$O5^{iii}$ is 2.809(2) Å. As a result, CuO_6 polyhedrons are grouped into flat tapes along the a parameter (Fig. 4), connecting with neighbors by four edges each.

In turn, the sodium ion is coordinated by seven oxygen atoms, two of which belong to water molecules (Fig. 5). The oxygen atoms are arranged such that four of them are separated by no more than 0.07 Å from the plane shown in Fig. 5. The angle between the normal to the plane and the line passing through the $O3^i$ and Na atoms is equal to 5.5°. The distances Na–O lie in the range 2.332(2) Å to 2.612(2) Å.

A water molecule is common for two Na ions. The Na–Ow–Na angle is equal to 93.8(1)° at the distances Na–O 2.342(3) and 2.441(3) Å. The positions of the hy-

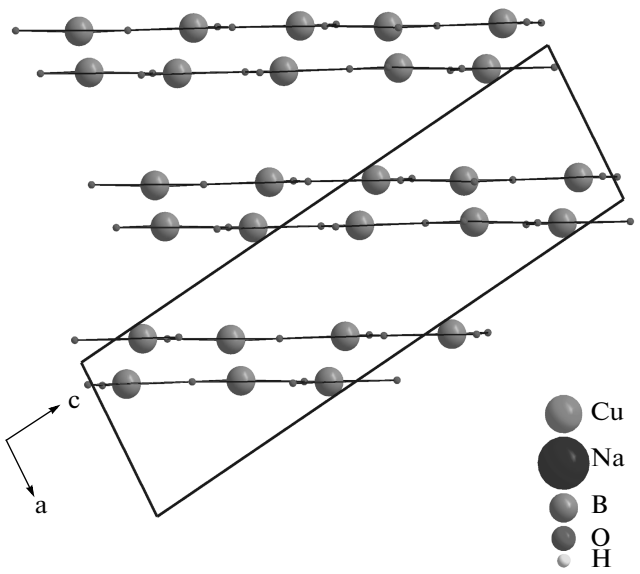

Fig. 2. Position of the planes of the BO_3 polyhedra in the structure of $CuNaB_3O_6 \cdot 0.842H_2O$. Not all atoms are shown

Table 2. Hydrogen link parameters in the $CuNaB_3O_6 \cdot 0.842H_2O$ crystal

Ow–H, Å	H–O6, Å	Ow ... O6, Å	Ow–H–O6	
0.97	2.47	3.297(3)	143°	$O6^{i}$
0.97	2.00	2.930(3)	161°	$O6^{ii}$

Note. i: $-x$, $y-1/2$, $1/2-z$; ii: x, $1/2-y$, $1/2+z$

drogen atoms are determined exactly. They are consistent with the positions determined from the electron density difference syntheses. As a result, there are hydrogen links O–H ... O in the crystal with the parameters listed in Table 2.

4. MAGNETIC MEASUREMENTS AND DISCUSSION

The magnetic measurements of the $CuNaB_3O_6 \cdot 0.842H_2O$ sample were performed using a SQUID magnetometer at $H = 300$ Oe in the temperature range 4.2–330 K. The sample consisted of a set of randomly oriented crystals, with a total mass of 85 mg. The temperature dependence of the magnetic susceptibility is presented in Fig. 6.

The magnetic susceptibility has a maximal value at $T = 330$ K $\chi_{max} = 3.1 \cdot 10^{-6}$ cm^3/g and decreases monotonically to a minimum at $T = 58$ K. An increase in the susceptibility occurs with a further decrease in the temperature, and is especially strongly pronounced in the temperature range 4.2 K $\leq T \leq$ 20 K.

The susceptibility does not follow the Curie–Weiss law in the entire temperature range, but the very small value of χ_{max} and its decrease with decreasing the temperature (see below) suggests that antiferromagnetic interactions dominate in the system.

The sharp increase in the susceptibility at low temperatures, in our opinion, is associated with the existence of small amounts of impurities or defects in the sample, which remains paramagnetic down to helium temperatures. With this assumption, the concentration of paramagnetic impurities $x \approx 10^{-2}$ was evaluated by least-square fitting of the experimental data in the temperature range 4.2 K $\leq T \leq$ 15 K by a $\chi = xC/T$ function, where x is the concentration of paramagnetic impurities and C is the Curie constant for the spin $S_{Cu} = 1/2$. The fitting curve and its difference from the experimental data are shown in Fig. 6.

The temperature behavior of the dependence of the magnetic susceptibility thus obtained is typical of systems with an energy gap between the ground nonmagnetic and excited states, the so-called spin-Peierls magnets [9–12]. The spin gap evaluation was performed by fitting the low-temperature region (up to $T = 150$ K) with the equation

$$\chi = \alpha \exp(-\Delta/k_B T) + \chi_0, \qquad (1)$$

where α is a constant that characterizes the dispersion of the exiting energy [6], Δ is the energy gap, and χ_0 is a constant term due to the diamagnetic contribution from the electron shell and Van Vleck paramagnetism. The solid curve in Fig. 6 shows the best fitting results with the parameters $\alpha = 8.26 \cdot 10^{-6}$, $\chi_0 = 4.99 \cdot 10^{-7}$ cm^3/g, and $\Delta/k_B = 259$ K.

Currently, there are several mechanisms for the formation of a spin-singlet ground state in these systems, namely, the interaction of spin and phonon subsystems [13], the charge [14–17] or orbital [18] ordering.

To clarify the mechanism of formation of a singlet ground state in $CuNaB_3O_6 \cdot 0.842H_2O$, it is necessary to consider the features of the crystal structure of this compound. Figure 7*a* shows the location of the copper ions in the $CuNaB_3O_6 \cdot 0.842H_2O$ structure, which form two linear chains, linked with each other, along the a axis of the crystal. Oxygen coordination octahedra in the chains are connected by edges, providing a 90-degree geometry links of the neighboring copper cations. These chains form a ladder of interconnected copper cations shown in Fig. 8.

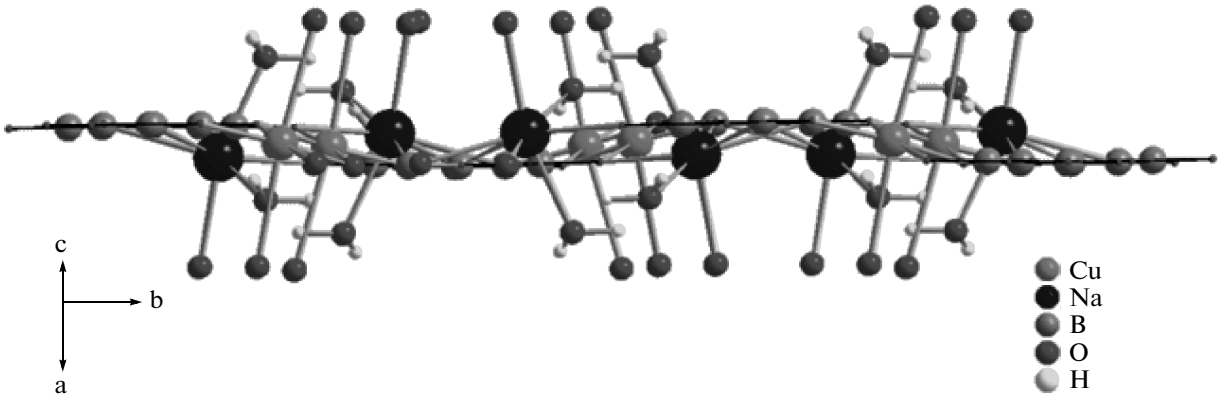

Fig. 3. Metal ion distribution in accordance with BO_3 planes in the $CuNaB_3O_6 \cdot 0.842H_2O$ crystal structure

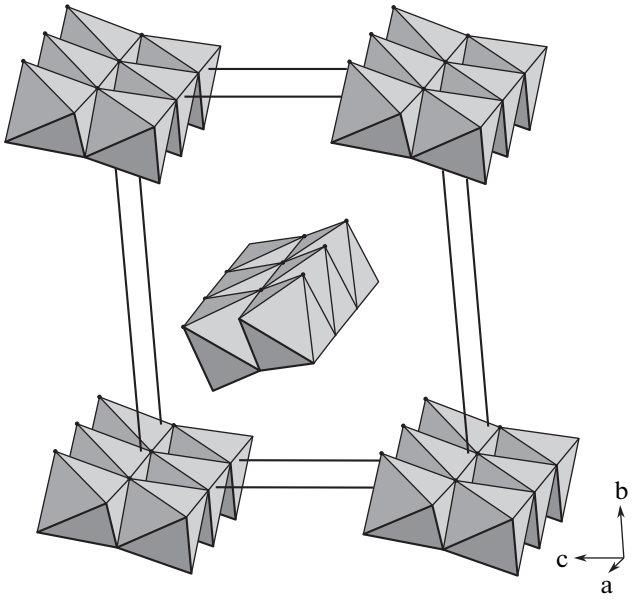

Fig. 4. Arrangement of CuO_6 polyhedra in $CuNaB_3O_6 \cdot 0.842H_2O$

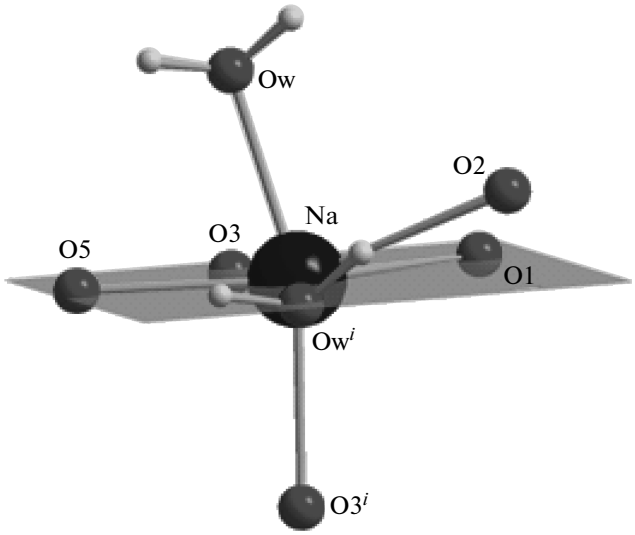

Fig. 5. Na^+ atom environment. The operation i changes the coordinate x to $x + 1$

We note that the Cu^{2+} ladders can be considered quasi-independent from each other, because they are "separated" from one another by extended O–Na–BO_3–O bridges. The oxygen octahedron has a strong tetragonal distortion (see Fig. 7*b*). The average ligand–cation distance in the basal plane of the octahedron is 1.925 Å, whereas the average ligand–cation distance along the long axis of the octahedron is 2.795 Å.

The singlet ground state can be formed due to the presence of Cu^{2+}ion pairs in the crystal structure, connected by strong antiferromagnetic exchange interaction.

We next discuss the population of 3*d*-orbitals of the Cu^{2+} ion in a tetragonal distorted oxygen octahedron with the Cu–O–Cu exchange interactions in the ladder. We consider the energy levels of the 3*d* electrons under the strong distortion of the ligand oxygen octahedron. Figure 9 shows a qualitative picture of the Cu^{2+} ion level splitting in the crystal fields of different symmetry.

Given the large tetragonal distortion of the oxygen octahedron, it may be assumed that the diagram of ion energy levels, in our case, is close to a flat square diagram. If we assume that the crystal field splitting of the energy levels E_d is comparable with the exchange field splitting, then an unpaired electron can be located at

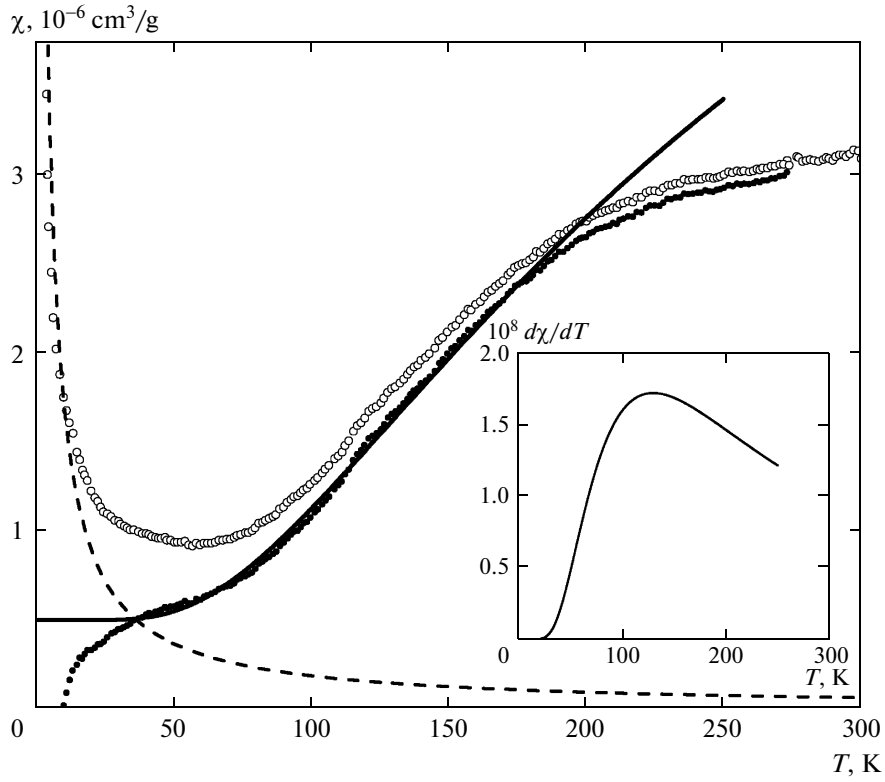

Fig. 6. Temperature dependence of the magnetic susceptibility for $CuNaB_3O_6 \cdot 0.842H_2O$. Open circles represent experimental data, the dotted line is the fitting curve $\chi = xC/T$, dark circles show the difference of the experimental and fitting curves. The solid curve is function (1), $\chi = \alpha \exp(-\Delta/k_BT) + \chi_0$. The inset is a derivative of function (1) with respect to the temperature

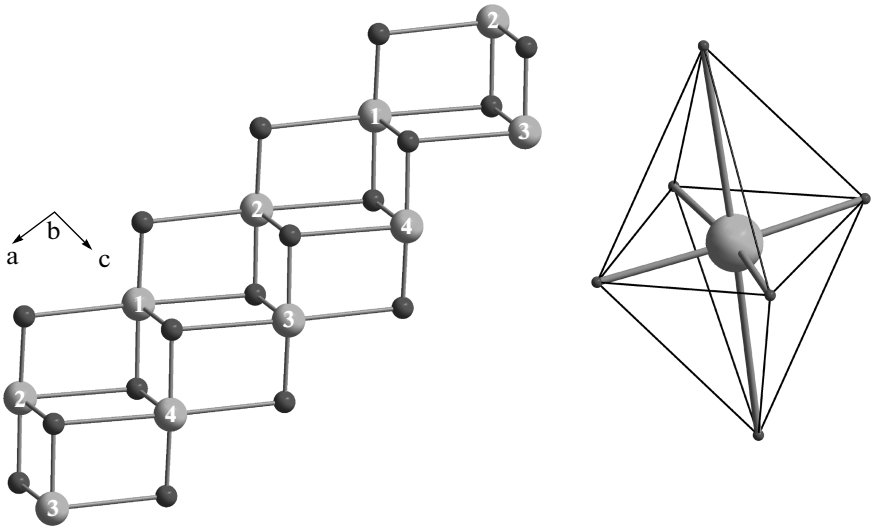

Fig. 7. *a*) Copper cations chains (large circles) in $CuNaB_3O_6 \cdot 0.842H_2O$. Small circles are coordination oxygen ions, *b*) oxygen octahedron

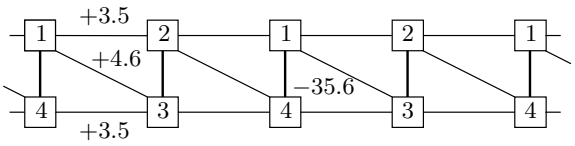

Fig. 8. Schematic representation of the linked chains of copper cations forming a ladder. Lines show the 90-degree exchange interactions, which strength will be evaluated in the text below

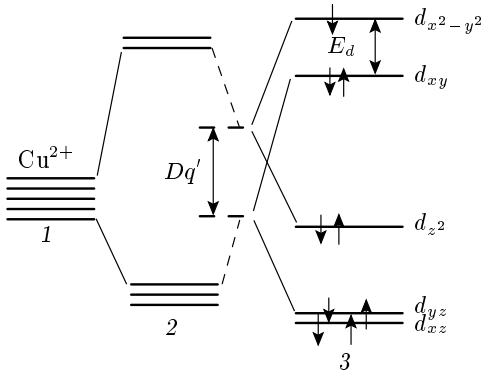

Fig. 9. Schematic diagram of the Cu^{2+} energy levels: *1* — free cation, *2* — regular octahedron, *3* — flat square [19]. Arrows represent the Cu^{2+} orbital population

any of the top ($d_{x^2-y^2}$ or d_{xy}) orbitals in Fig. 9. Under this assumption, there are three possibilities of indirect exchange interaction between the copper ions.

The first one is when the $d_{x^2-y^2}$ orbitals of all copper ions are populated; the indirect exchange interaction model [20] then gives two values of the exchange parameters in a ladder:

$J_{12,13,24,34}(d_{x^2-y^2}, d_{x^2-y^2}) = +4bcJ^{int} \approx +9.3$ K for the short axis of the octahedron, and

$J_{14,23}(d_{x^2-y^2}, d_{x^2-y^2}) < +2bcJ^{int} < +4.6$ K for the long axis of the octahedron.

In the formulas, exchange indexes denote the number of the magnetic sublattice in accordance with Figs. 7 and 8, J^{int} is the intra-atomic interaction integral, $b = \gamma^2$ is the ligand–cation transport parameter on a σ-bond, c is the ligand–cation transport parameter on a π-bond, and γ is the covalency bond parameter. For the oxide compounds with the ligand–cation distances about 2 Å, $b \approx 0.02$, $c \approx 0.01$, and $J^{int} \sim 1$ eV [20]. Next to the formulas, estimations of the parameters of pair exchange interaction in Kelvins are given. It is clear that the positivity of all pair exchange interactions in this ladder leads to the ferromagnetic ground state of the system with the exchange field at a cation about 12.5 K.

Table 3. Indirect sublattice exchange interactions in $CuNaB_3O_6 \cdot 0.842H_2O$

zJ_{ij}, K	1 ↑	2 ↑	3 ↓	4 ↓	E_e, K
1 ↑	0	**+7.0**	*+4.6*	**−35.6**	19
2 ↑	**+7.0**	0	**−35.6**	*+4.6*	19
3 ↓	*+4.6*	**−35.6**	0	**+7.0**	19
4 ↓	**−35.6**	*+4.6*	**+7.0**	0	19

The second possibility is when the unpaired electrons of all Cu^{2+} ions are located on d_{xy} orbitals; as in first case, we then obtain two values for the exchange parameters:

$J_{12,13,24,34}(d_{xy}, d_{xy}) = +(22/3)bcJ^{int} \approx +17$ K for the short axis of the octahedron, and

$J_{14,23}(d_{xy}, d_{xy}) < +2c^2J^{int} < +2.3$ K for the long axis of the octahedron.

Again, we have a ferromagnetic ground state with the exchange field at a cation about 12.5 K.

The third case is where an unpaired electron is located on the $d_{x^2-y^2}$ orbital of one Cu^{2+} ion and on the d_{xy} orbital of the neighboring Cu^{2+} ion; the spin ordering in ladder is then governed by three exchange parameters:

$J_{14,23} = -2bc(2U - (1/3)J^{int}) \approx -35.6$ K for the short axis of the octahedron and

$J_{12,34} < +c(b + c)J^{int} < +3.5$ K,

$J_{13,24} < +2bcJ^{int} < +4.6$ K for the long axis of the octahedron.

Here, U is the energy of the ligand–cation electron excitation. Its value can be 2–6 eV in oxide compounds [20]. In our calculations, $U = 4$ eV.

In the third case, interactions in the ladder can be characterized by the exchange parameters for the four-sublattice system listed in Table 3.

The arrows show the orientation of the sublattice magnetic moments due to the existing exchange interactions. Frustrated interactions are shown with the italic font. In the last column, the exchange fields acting on each copper cation are given. Such an orbital occupation leads to orbital ordering.

We note that the exchange fields acting on the copper cations in the case of orbital ordering (case 3) (19 K) are greater than those in the first two cases (12 K). In accordance with the choice of the lowest-energy ground state, the system would prefer the ordering shown in Table 3. That is, electrons of neighboring Cu^{2+} ions would be located on different orbitals when

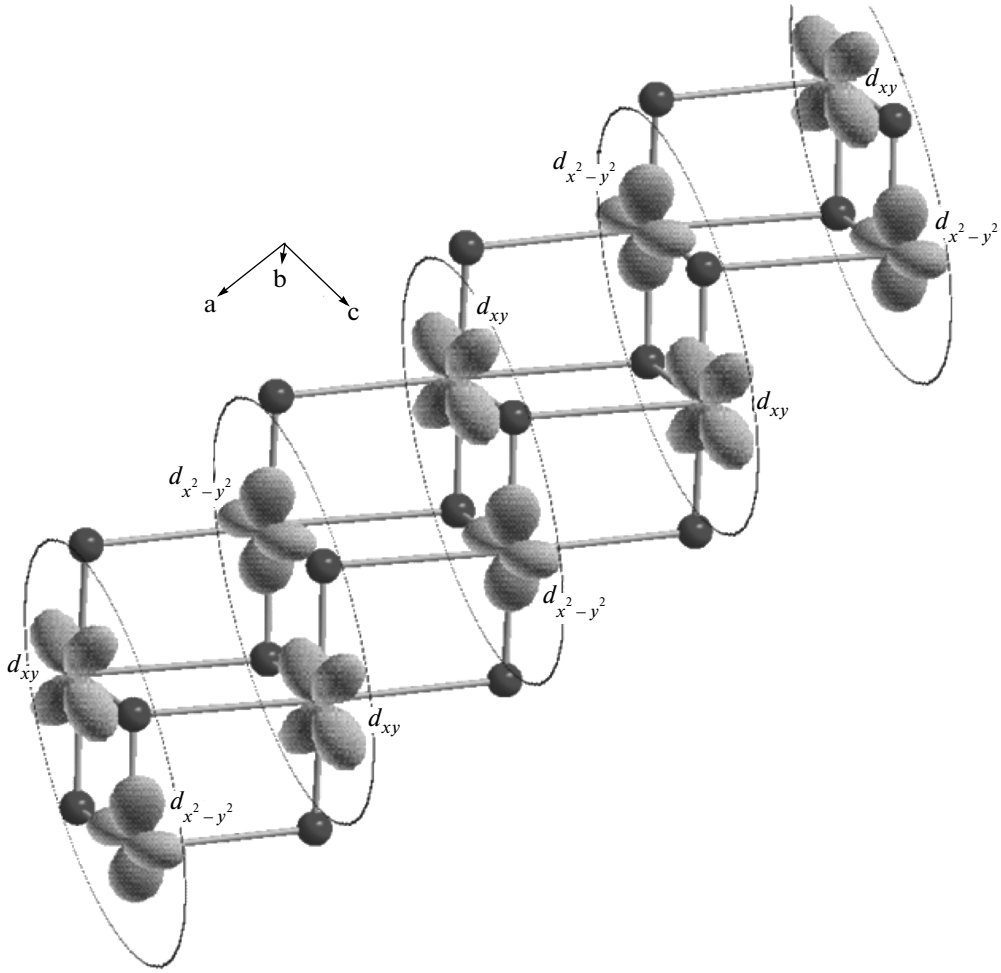

Fig. 10. Type of orbital ordering of the Cu^{2+} ladder in $CuNaB_3O_6 \cdot 0.842H_2O$. The ion symbols are the same as in Fig. 7

the energy of the exchange interaction E_e of the pairs of neighboring cations is comparable to the splitting E_d of the $d_{x^2-y^2}$ and d_{xy} orbitals in the crystalline field.

Hence, the strong pair antiferromagnetic interaction (-36 K) together with the weak inter-pair interaction ($+3.5$ K and, in the frustrated case, $+4.6$ K) are the main mechanisms leading to the singlet ground state of the system. The proposed picture of orbital ordering in the ladder is shown in Fig. 10.

It is well known that ladder systems can have a singlet ground state without orbital ordering under some circumstances, namely, for $J_{NN} < 4J_{NNN}$ and $J_{NN} < 0$, where J_{NN} and J_{NNN} are the nearest-neighbor and next-nearest-neighbor exchange interactions, respectively. In our case (see cases 1 and 2), this is not satisfied however.

The spin-Peierls transition temperature can be estimated from the $d\chi/dT$ curve, the inset in Fig. 6, as $T_{SP} \sim 128$ K. In addition to the formation of the ground nonmagnetic state, orbital ordering can also lead to the doubling of the lattice along the a axis at low temperatures and to the structural phase transition at an increased temperature.

4.1. Magnetic resonance

Magnetic resonance spectra were collected with a Bruker Elexsys E580 (X-band) spectrometer at temperatures 110 K $\leq T \leq$ 410 K with the 100 kHz modulation frequency. The sample contained a set of randomly oriented single crystals with a mass about 100 mg.

The temperature evolution of the resonance spectra is shown in Fig. 11.

The spectrum of a magnetic resonance consists of several signals. The first is well observed at all temperatures in the field about 3000 Oe and has the linewidth

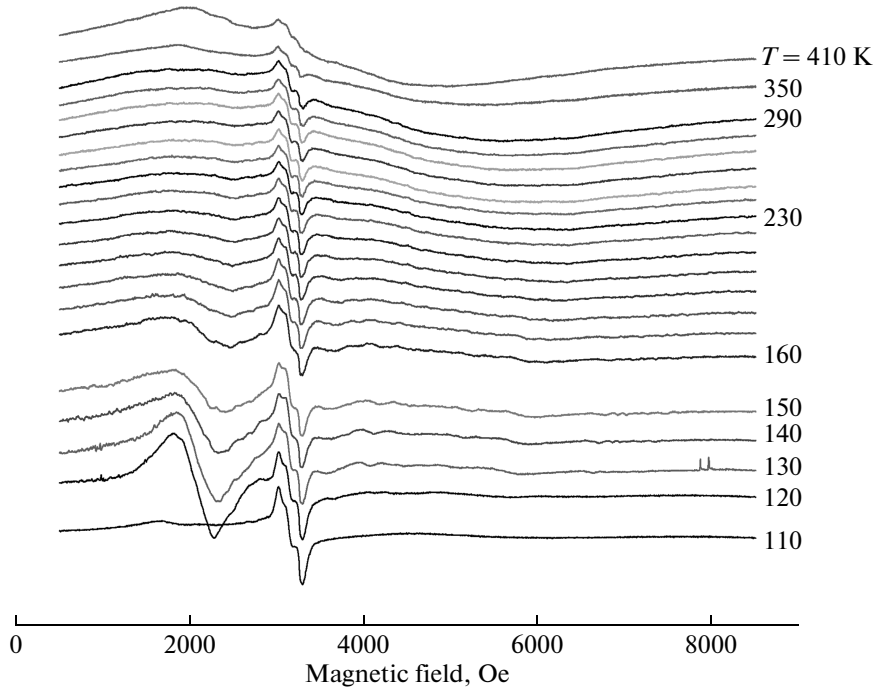

Fig. 11. Temperature evolution of the resonance spectra in $CuNaB_3O_6 \cdot 0.842H_2O$

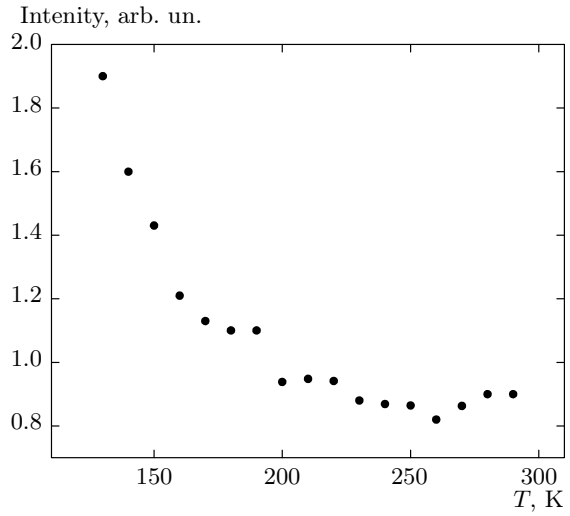

Fig. 12. Temperature dependence of the integrated intensity of the signal in the field about 3000 Oe

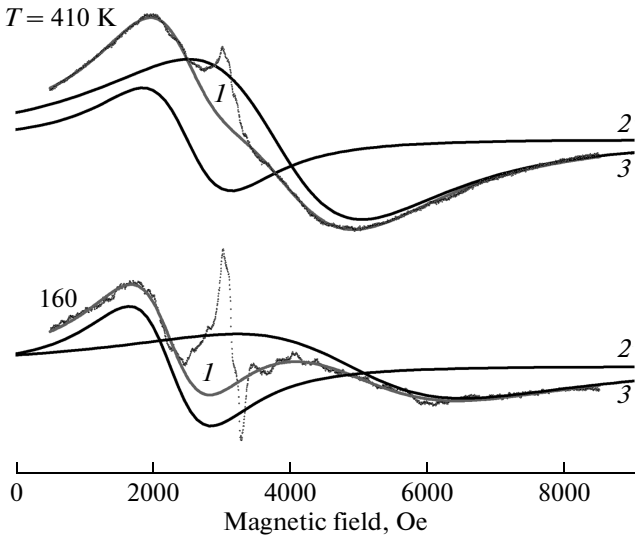

Fig. 13. Computer simulation of the second signal in the $CuNaB_3O_6 \cdot 0.842H_2O$ spectrum. Points are the experimental spectrum, solid lines are as follows: *1*, resultant signal, *2* and *3*, modeling Lorentzian lines

about 300 Oe. The second is broad at room temperatures and strongly changes below $T \leq 160$ K.

The first signal, in our opinion, belongs to an uncontrollable magnetic impurity in the sample, because its integrated intensity is two orders less than the basic wide signal. Besides, the temperature dependence of its integrated intensity (see Fig. 12) is typical for paramagnets and does not correlate with the temperature dependence of the magnetic susceptibility of the entire

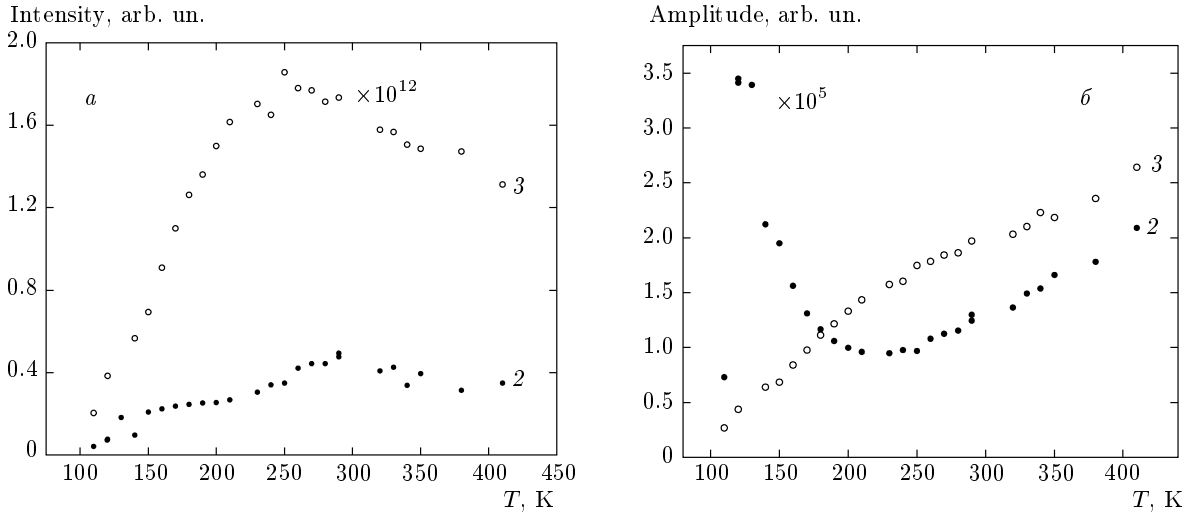

Fig. 14. Temperature dependence of *a*) the integrated intensities and *b*) the amplitudes for lines *2* and *3* from Fig. 13

sample (see Fig. 6). Apparently, the sharp increase in magnetic susceptibility at temperatures below 15 K is due to the presence of impurities in the sample.

Computer simulations showed that the second broad signal represents a superposition of two Lorentzian shape lines, as shown in Fig. 13.

To confirm the assumption about the singlet ground state of the magnetic system $CuNaB_3O_6 \cdot 0.842H_2O$, the temperature dependence (Fig. 14) of the integrated intensities of lines *2* and *3*, defined as the product $A(T) \cdot \Delta H^2(T)$, where A is the amplitude of the signal and ΔH is the line width (peak-to-peak), were calculated.

The integrated intensities of lines *2* and *3* reach a maximum at the respective temperatures 300 K and 250 K, and decrease as the temperature decreases. Both signals disappear at $T < 100$ K. Such behavior is typical of the system with the singlet $S = 0$ ground state. The abrupt change of the amplitude of line *2* at the temperature $T \approx 120$ K is very pronounced. This temperature is very close to the spin-Peierls transition temperature $T_{SP} \sim 128$ K estimated from the temperature dependence of the magnetic susceptibility (see above). This anomalous behavior of the amplitude of the signal can, in our opinion, be an indication of a structural phase transition in $CuNaB_3O_6 \cdot 0.842H_2O$ at $T = T_{SP} \sim 128$ K. At present, it is not clear whether two signals are present in the magnetic resonance spectrum.

To check the existence of the structural phase transition, the specific heat and Raman scattering measurements were carried out in the temperature range 78 K $< T <$ 300 K. We note that only a slight anomaly was observed in the specific heat vs. temperature dependence at $T = 103$ K, with no changes in the Raman spectra. It seems that the slight anomaly in the specific heat is too small and is not similar to those observed at typical structural phase transitions. To clarify this uncertainty, growing large single crystals of high quality is in progress.

5. CONCLUSION

The new compound $CuNaB_3O_6 \cdot 0.842H_2O$ was grown for the first time. Its space group and atomic coordinates were determined. It was proposed that the system undergoes a magnetic phase transition of the spin-Peierls type to the singlet ground state at $T_{SP} \sim 128$ K. The energy gap between the ground ($S = 0$) and exited ($S = 1$) states was determined as $\Delta/k_B = 259$ K. The existence of a structural phase transition at $T = T_{SP} \sim 128$ K was suggested. In order to perform a detailed investigation, growing large high-quality crystals is in progress.

REFERENCES

1. G. A. Petrakovskii, K. A. Sablina, A. M. Vorotynov et al., JETP **71**, 772 (1990).

2. M. Hase, I. Terasaki, and K. Uchinokura, Phys. Rev. Lett. **70**, 23 (1993).

3. G. A. Petrakovskii, Russtan Physics Journal **41**, 1 (1998).

4. A. M. Vorotynov, A. I. Pankrats, G. A. Petrakovskii, and K. A. Sablina, JETP **86**, 5 (1998).

5. G. A. Petrakovskii, K. A. Sablina, A. I. Pankrats et al., J. Magn. Magn. Mater. **140–144**, 1991 (1995).

6. G. A. Petrakovskii, K. A. Aleksandrov, L. N. Bezmaternikh et al., Phys. Rev. B **63**, 184425 (2001).

7. Bruker APEX 2 and SAINT. Bruker AXS Inc., Madison, Wisconsin (2008).

8. G. M. Sheldrick, Acta Cryst. A **64**, 112 (2008).

9. M. Hase, I. Terasaki, and K. Uchinocura, Phys. Rev. Lett. **70**, 3651 (1993).

10. J. W. Brag, H. R. Hart, L. V. Interrante, I. S. Jacobs, J. C. Kasper, G. D. Watkins, and S. H. Wee, Phys. Rev. Lett. **35**, 11 (1975).

11. S. Huzinga, J. Kommander, G. A. Sawatzky, B. T. Jhole, K. Kopinga, and W. J. M. DeJonge, J. Roos. Phys. Rev. B **19**, 9 (1979).

12. Masahiko Isobe, Emi Ninomiya, Alexander N. Vasil'ev, and Yutaka Ueda, J. Phys. Soc. Jpn. **71**, 6 (2002).

13. T. Rytte, Phys. Rev. B **10**, 11 (1974).

14. T. Ohama, H. Yasuoka, M. Isobe, and Y. Ueda, Phys. Rev. B **59**, 3299 (1999).

15. H. Seo and H. Fukuyama, J. Phys. Soc. Jpn. **67**, 2602 (1998).

16. K. Ohwada, Y. Fujii, N. Takesue, M. Isobe, Y. Ueda, H. Nakao, Y. Wakabayashi, Y. Murakami, K. Ito, Y. Amemiya, H. Fujihisa, K. Aoki, T. Shobu, Y. Noda, and N. Ikeda, Phys. Rev. Lett. **87**, 086402 (2001).

17. H. Sawa, E. Ninomiya, T. Ohama, H. Nakao, K. Ohwada, Y. Murakami, Y. Fujii, Y. Noda, M. Isobe, and Y. Ueda, J. Phys. Soc. Jpn. **71**, 385 (2002).

18. O. A. Bayukov, G. A. Petrakovski, and A. F. Savitski, Phys. Sol. St. **40**, 9 (1998).

19. I. B. Bersuker, *Elektronnoe Stroenie i Svoistva Koordinacionnyh Soedinenii*, izd. "Himia", Leningradskoe otd. (1976).

20. O. A. Bayukov and A. F. Savitski, Phys. Sol. St. **36**, 7 (1994).